CrossMark

Studies on properties of as-synthesized conducting polythiophene through aqueous chemical route

N. S. Wadatkar[1] · S. A. Waghuley[2]

Abstract In this research article, as-synthesized polythiophene (PTh) were analyzed through FTIR, XRD, FESEM and TG/DTA techniques. The polymerization of PTh were confirmed through FTIR and XRD analysis. The temperature dependence of DC electrical conductivity of the samples has been obtained over a temperature range from 303 to 393 K followed Arrhenius relation. The DC conductivity of the samples was found to be in the range of 10^{-6}–10^{-4} S cm^{-1}. The activation energies of the samples were ranges between 0.23 and 0.14 eV. The variation of AC electrical conductivity with frequency obeys Jonscher power law. Moreover, dielectric studies were made using AC impedance analyzer in the frequency and temperature ranges 20 Hz–1 MHz and 303–393 K, respectively. The maximum value of DC conductivity was found to be 2.14×10^{-4} S cm^{-1} at 348 K for PTh with stoichiometric ratio (70:30) wt% of thiophene and FeCl$_3$, which increases with temperature.

1 Introduction

Recently, conjugated conducting polymers founds great applications in a variety of new areas, such as sensors [1], rechargeable batteries [2, 3], capacitors [4], supercapacitors [5, 6], fuel cells [7], light emitting diode [8], and photovoltaic devices [9], etc. The typical conducting polymers consist of polyaniline (PANi), polypyrrole (PPy), polythiophene (PTh), and their derivatives. The conducting polymers have most advantageous properties such as good thermal and environmental stability, corrosion protection of metallic electrodes, easy method of preparations [10]. The most common types of conducting polymers in their neutral states are insulators referred to as conjugated polymers. However, chemical or electrochemical treatment to such conjugated polymers with oxidants followed by anion intercalation can result in the formation of semiconductive or conductive states [11].

Among various studied conducting polymers, PTh is extremely thermally stable organic conducting polymer [11, 12]. Therefore, PTh is one of the most widely studied of all conjugated conducting polymers. There are numerous methods for synthesizing polymer, which will be remodelled into conductive polymers; the incorporation of extended p-electron conjugation is of foremost importance [13]. Normally, polymerization will be achieved by chemical or electrochemical processes, which offer, samples with different morphologies and consequently slightly different physical and chemical properties [14]. The synthesis conditions and also the nature of the dopant anion play a vital role within the polymerization process [15, 16]. The available literature disclosed completely different methods for the synthesis of PTh like chemical [17], electrochemical [18], photochemical [19], ultrasonic assisted [20], etc. The nanoparticles of PTh has been synthesized via Fe^{3+}-catalyzed oxidative polymerization of unsubstituted thiophene monomers in aqueous dispersion [21]. PTh has been chemically synthesized, undoped using aqueous ammonia and then re-doped using FeCl$_3$ as well as iodine [22]. PTh containing 3,4-ethylenedioxythiophene in a repeat unit was firstly derived by electro polymerization of the corresponding monomer in acetonitrile. The polymer

✉ S. A. Waghuley
  sandeepwaghuley@sgbau.ac.in

1   Department of Physics, Government Polytechnic, Yavatmal 445001, India

2   Department of Physics, Sant Gadge Baba Amravati University, Amravati 444 602, India

film showed high electrical conductivity comparable to PTh and poly(methylthiophene) despite of its short π-conjugation length [23]. Film shows surface phenomena, where π-orbitals can easily delocalised, which results in high electrical conductivity. The electrical conductivity of PTh has been enhanced by surfactant additives, the highest value for PTh with Tween 20 was reported to be 4.6×10^{-4} S cm^{-1} [24]. In an iodine doped PTh with same crystallinity or even higher than undoped sample, DC conductivity will further increase. Bipolarons are responsible for increase in DC conductivity of PTh, when doped with iodine [25]. Recently, it was reported that the optimum conditions were explored to prepare the single-phase product with a composition of $Li_{0.12}(PTP)_{0.54}MoS_2$. The nanocomposite exhibits enhanced electrical conductivity in the order of 10^{-2} S cm^{-1} at ambient temperature, resulted from the incorporation of the electronically conductive PTh between the semiconducting host layers and the coupling between the guest conjugated p-orbits and the host layers [26].

This research article is intended by presenting a more systematic report on the novel one pot synthesis of conducting PTh through chemical oxidative route at room temperature. The samples of PTh are synthesized with FeCl$_3$ as an oxidant in aqueous solution in the form of pellets. In this manuscript we unified reports the thermal, electrical and dielectric properties of as-synthesized samples of PTh. Moreover, infrared (FTIR) and X-ray diffraction (XRD) techniques verified the existence of PTh chains in as-synthesized materials, field effect scanning electron microscopy (FESEM) was used to determine the morphology, whereas thermo gravimetric/differential thermal analysis (TG/DTA) was employed to study thermal properties of derived polymeric materials.

## 2 Experimental

2.1 Synthesis of PTh

All chemicals, such as monomer thiophene, oxidant anhydrous iron (III) chloride (FeCl$_3$), 0.1 M of hydrogen peroxide (H$_2$O$_2$) used as catalyst, were of analytical grade and procured from SD Fine Chemicals, India. The thiophene monomer was used as received for synthesis of PTh without further purification. The sample was synthesized at room temperature (303 K) by mixing monomer with FeCl$_3$ in deionised water. The H$_2$O$_2$ was used to enhance the rate of reaction and also yield. After the rigorous stirring, drop-by-drop monomer was added into the solution. The preliminary polymerization process was identified by the colour change (brown) of the reaction mixture. The polymerization process was allowed for constant stirring for 8 h with a magnetic stirrer at 30 °C. The resulting precipitate was collected by vacuum filtration using cellulose nitrate filter papers. The precipitate was washed with copious amounts of triply distilled water until the washings were clear and then kept for overnight at room temperature. Subsequent to this step, samples were sintered at 60 °C for 30 min. In this way, different samples of PTh were synthesized by varying the stoichiometric ratios of thiophene and FeCl$_3$ as 90:10, 80:20, 70:30, 60:40 and 50:50 wt%.

The chemical oxidative polymerization method is generally used for the synthesis of conducting polymeric compound from various classes of monomers like aniline, thiophene, pyrrole, etc. In oxidative polymerization method, the monomer is characterized by electron donor properties and high oxidation tendency due to presence of electron donor substituent in benzene or heterocyclic ring [27]. The oxidative polymerization of monomer takes place under the action of inorganic or organic oxidizing agent. Normally, metal chloride is used as an oxidizing agent. The cation or cation radical sites are generated in monomer during this process, so formation of covalent bond between monomer molecules and monomer form the chain structure [28]. During the chemical polymerization, temperature of the process generally increases. The majority of oxidative polymerization reactions are exothermic. Scheme 1 shows that mechanism involves in the chemical oxidative polymerization of PTh.

2.2 Materials characterization

The physico-chemical and thermal properties of as-synthesized samples were characterized through FTIR, FESEM, and TG/DTA techniques. The FTIR spectrum was recorded on Shimadzu (Model-8201) spectrophotometer. The FTIR was taken in the KBr medium at room temperature in the region 4000–400 cm^{-1} at scan rate 16. The structure, morphology and grain size of the samples were reported from FESEM (JEOL JSM-6360). The TG/DTA was carried out on Shimadzu DTG-60 h thermal analyzer under nitrogen flow at the heating rate of 10 °C/min. The temperature of the sample was varied from room temperature to 873 K. The AC impedance measurements were performed through LCR meter, Agilent Technology, Singapore, in a frequency region of 20 Hz–1 MHz and a temperature range of 303–393 K. For electrical measurement, the as-synthesized polymeric samples were fabricated in the form of pellets through KBr Press (0–15 Tons). The values of diameter and thickness of all the five pellets were same, which were found to be 0.738 and 0.186 cm, respectively. In order to study electrical parameters, silver electrodes are used.

Scheme 1 Mechanism of chemical polymerization of PTh
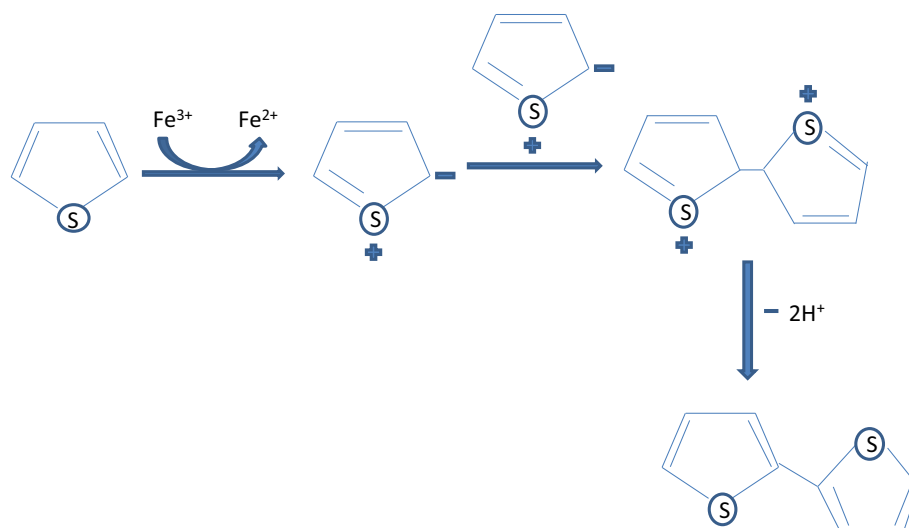
3 Results and discussion

3.1 FTIR analysis

FTIR spectroscopy has been employed to analyze the interactions among atoms or ions in the structure. Figure 1 depicts the FTIR spectra of PTh powder samples with different wt% of thiophene and $FeCl_3$ (a) 90:10, (b) 80:20, (c) 70:30, (d) 60:40 and (e) 50:50 in the wave number range 400–4000 cm^{-1}. The spectrum showed the (C–S)
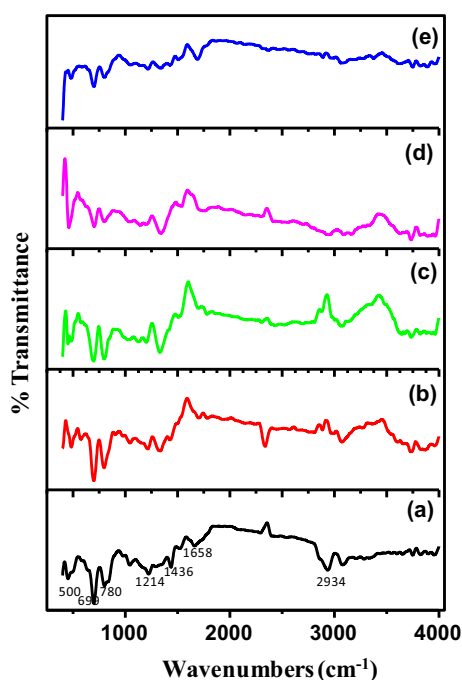

Fig. 1 FTIR spectrum of PTh samples with different wt% of thiophene and $FeCl_3$ as (*a*) 90:10, (*b*) 80:20, (*c*) 70:30, (*d*) 60:40 and (*e*) 50:50

bending band at 780 cm^{-1}; (C–H) bending band at 1214 cm^{-1} [24]; the bands at 1658 and 1436 cm^{-1} represents the (C=C) symmetric and (C=C) asymmetric vibrating modes in the thiophene ring [29] and (C–H) stretching vibration band at 2934 cm^{-1} [22]. The major peak at 500 cm^{-1} to the presence of C=C in PTh. The band at 699 cm^{-1} represents C–S–C ring deformation which appears with a shoulder peak due to increase in oxidant concentration [24]. The weaker feature in the range 1030–1018 cm^{-1} corresponds to (C–C stretching + C–H wagging components) [29]. The doping induced band at 1021 cm^{-1} was originating from the changes in the conjugated backbone due to the electron withdrawing and electron donating dopants on the polymer chain and the counter ion balancing appeared at 1045, 1342 and 1436 cm^{-1} [30]. The slight shifting of peaks may be due to different concentration of $FeCl_3$. The large descending base line in the spectral region of 4000–2000 cm^{-1} was attributed due to free-electron conduction in the doped polymer.

This type of behaviour was not observed in undoped polymer. The increasing conjugation shifted the absorption frequencies of the polymer. These results are supported to the polymerization.

3.2 XRD analysis

Figure 2 depicts the XRD patterns of the samples of PTh with different stoichiometric ratios of thiophene and $FeCl_3$ as (90:10–50:50) respectively. The XRD patterns of the samples of PTh are amorphous in nature. In each case, broad peaks are observed at about $2\theta = 18°$, 18.1°, 18.16°, 18.12° and 18.08° (Fig. 2a–e). The broad peaks represent the characteristic of amorphous PTh [31] and are due to the scattering from PTh chains at the interplanar spacing. However, the position of the maximum intensity of the
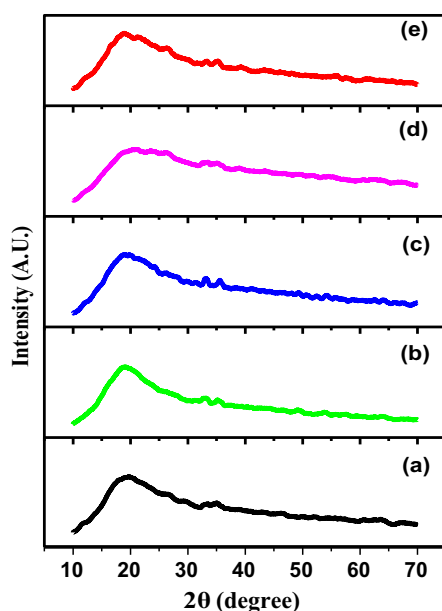
Fig. 2 XRD pattern of PTh samples with different wt% of thiophene and FeCl$_3$ as (*a*) 90:10, (*b*) 80:20, (*c*) 70:30, (*d*) 60:40 and (*e*) 50:50

Fig. 3 FE-SEM picture of PTh with (70:30) wt% of thiophene and FeCl$_3$

amorphous halos is different from each other for each sample. It may be interested to note that the peak position of these amorphous halos depends on the concentration of oxidant. The average chain separation can be calculated from these maxima using the relation [32].

$$R = 5\lambda/8 \sin \theta \tag{1}$$

where R is the polymer chain separation, λ is wavelength of X-ray source and θ is the diffraction angle at the maximum intensity of amorphous halo. The average chain separation (R) was found to be 2.62, 2.77, 2.44, 2.56, and 2.69 Å for PTh with different stoichiometric ratios of thiophene and FeCl$_3$ as 90:10, 80:20, 70:30, 60:40 and 50:50 wt%, respectively.

3.3 Morphological investigation

The typical morphology of PTh powder derived by chemical polymerization method was investigated by using FESEM image. Figure 3 shows the surface morphology of PTh with stiochometric ratio (70:30) wt% of thiophene and FeCl$_3$. The FESEM image shows the spongy and fibril structure with 2.5 μm size. The phases present in the micrograph due to Cl ions that remained as a dopant in PTh. The micrograph shows irregular shape and size due aggregation up to some extent as well as an agglomeration of particles.

3.4 TG/DTA analysis

Thermogravimetry is the most widely used tool to characterize the thermal decomposition of polymers. The typical TG curves of normalized weight and derivative
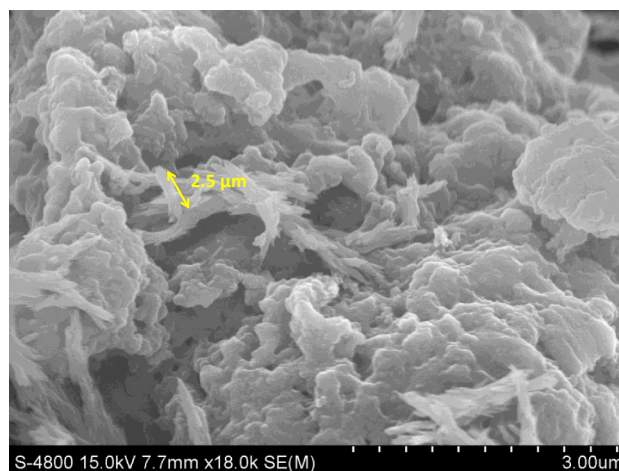
thermogravimetry (DTG) data of the derivative weight of PTh with stoichiometric ratios (80:20, 70:30, 60:40) wt% of thiophene and FeCl$_3$ are plotted as a function of temperature in Fig. 4a–c respectively. All the DTG curves illustrate that the decomposition process is a single-step. In all three cases, there exists exotherm at 350 K which is due to the elimination of dopant.

Thermal decomposition reaction of PTh with 80:20 wt% of thiophene and FeCl$_3$ was observed at 479 K and end at 746 K with maximum rate of degradation at 605.15 K. TGA (Fig. 4a) shows three weight-loss steps. The first step (313–479 K) is attributed to the evaporation of adsorbed water molecules on the sample surface. The adsorbed water amount is less than 6 %. The second weight-loss step from about 479–746 K is complicated. This is attributed to the loss of dopant anions bound to the PTh chain. The third step weight loss occurs between 746 and 1023 K. This last step is due to the skeletal PTh backbone chain structure [33]. At the end, i.e. at 1023 K, the total loss is nearly 68 %. In Fig. 4b, the thermal decomposition reaction of PTh with 70:30 wt% of thiophene and FeCl$_3$ was observed at 469 K and end at 721 K with maximum rate of degradation at 595.15 K, whereas TGA shows, the weight loss up to 469 K is about 5 %, which is due to loss of water molecules. The second weight-loss step occurs between 469 and 721 K. The third step lies between 721 and 1023 K. The total weight loss is about 63 %. In case of PTh with 60:40 wt% of thiophene and FeCl$_3$ (Fig. 4c), thermal decomposition reaction was observed between 425 and 710 K with maximum rate of degradation at 601.58 K. TGA shows 6 % weight loss between 313 and 425 K could be due to moisture trapped in the polymer. Within the temperature range 425 and 681 K, the prominent weight loss is observed. The third degradation step occurs between 681 and 1023 K. At the end, total weight loss is about
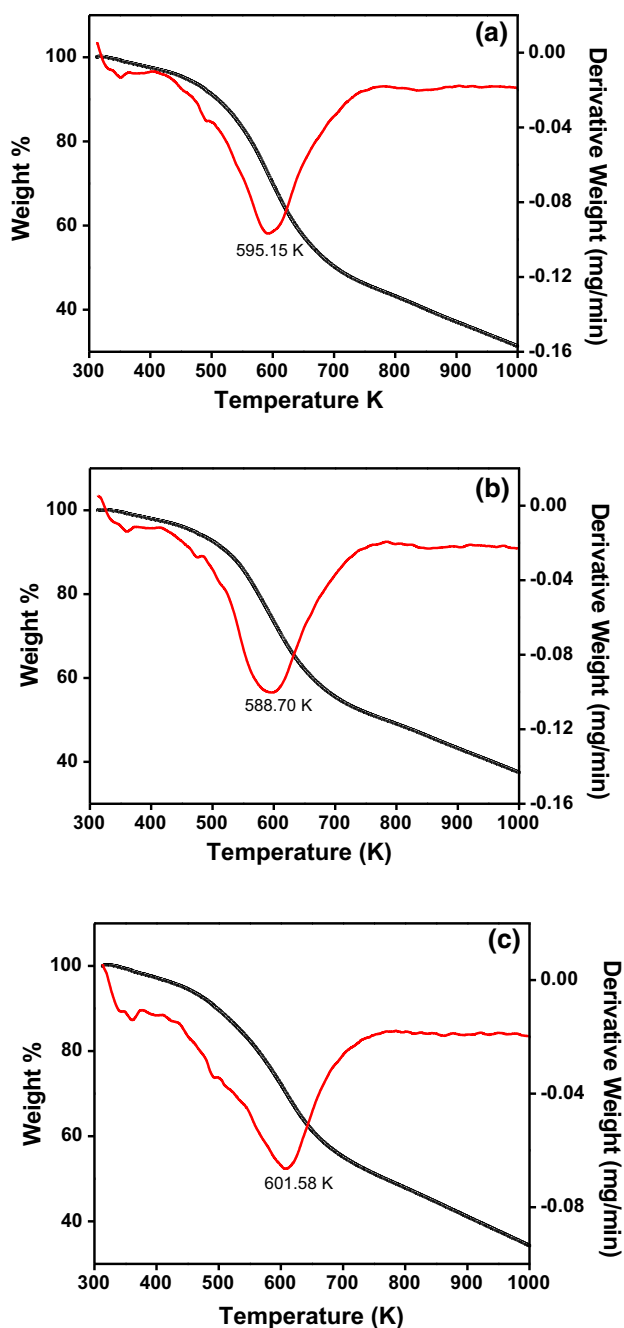
Fig. 4 TGA-DTG curves for PTh with **a** 80:20, **b** 70:30 and **c** 60:40 wt% of thiophene and FeCl$_3$

70 %. Thus, it is concluded that, the thermal properties of PTh as-synthesized using an oxidant FeCl$_3$ have been more stable [34].

3.5 Impedance analysis

Figure 5 depicts the complex impedance plot of as-synthesized samples of PTh at 348 K. The Z″ versus Z′ impedance spectra represent that the semicircles are

depressed and their centres are shifted down to the real axis, which indicates the distribution of relaxation time [35].

Furthermore, the diameter and the maximum of semicircles for all samples decrease with increase in temperature, indicating an activated conduction mechanism [36]. The same plot of PTh with stoichiometric ratio (70:30) wt% of thiophene and FeCl$_3$ at different temperatures is as shown in Fig. 6.

3.6 Temperature dependent conductivity

Figure 7 shows the variation of Ln σ with inverse absolute temperature of PTh with different stoichiometric ratios of thiophene: FeCl$_3$ (90:10–50:50). From the plot, it is observed that the conductivity of PTh samples does not show any abrupt jump with temperature, indicating that PTh samples exhibit a completely amorphous structure. PTh with a stoichiometric ratio of thiophene: FeCl$_3$ (70:30) wt% shows optimum conductivity. This may be due to the fact that extent of polymerization may be more rather than other ratios, so that there may be more bipolarons available for electrical conductivity. The optimum value of DC conductivity may be due to least value of polymer chain separation of respective sample. The least value of polymer chain separation results in effective hopping mechanism. The ionic conductivity increases with increase in temperature for all the samples and this behaviour is in agreement with the theory [37]. The ionic transport mechanism interpreted the enhancement of the ionic mobility involving coordinating sites, local structural relaxations and segmental motion of the polymer chain in a free volume model [38].

The activation energies were estimated from Ln σ versus 1000/T plots (Fig. 8) using the Arrhenius relation.
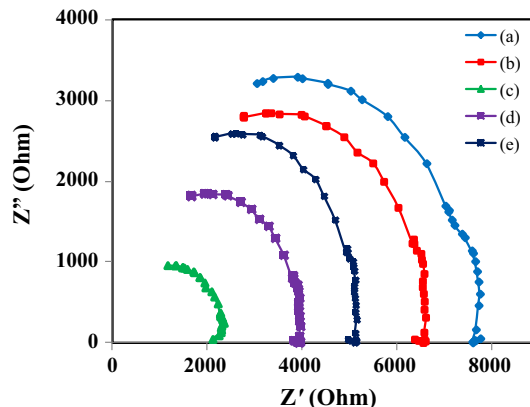
$$\sigma = \sigma_0 \exp(-E_a/kT) \qquad (2)$$

Fig. 5 Cole-cole plot for as-synthesized samples of PTh at 348 K
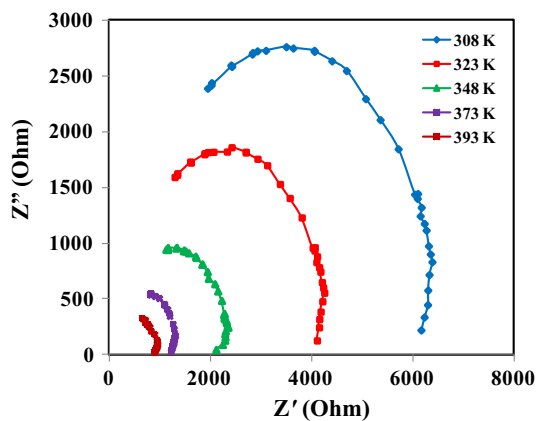
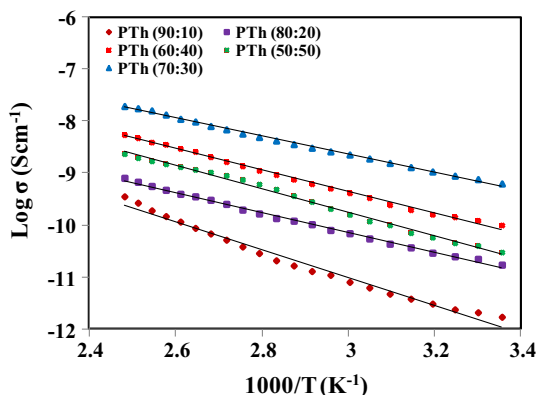**Fig. 6** Cole-cole plot of PTh for (70:30) wt% of thiophene and FeCl$_3$

Fig. 7 Arrhenius plot for PTh with different stoichiometric ratios of thiophene and FeCl$_3$

where, σ_0 is a constant, E_a, the activation energy, k, the Boltzmann constant and T, the absolute temperature. The activation energy, E_a was calculated from the least square straight line fitting of plot. The DC conductivity values for
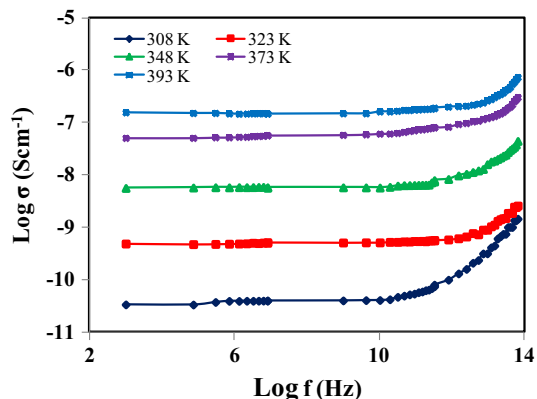

Fig. 8 Frequency and temperature dependence conductivity plot of PTh for (70:30) wt% of thiophene and FeCl$_3$

the all the samples of PTh can be estimated from the impedance. The values of DC conductivity σ and activation energy E_a for PTh with different stoichiometric ratios of thiophene and FeCl$_3$ are given in Table 1. Activation energy and the slopes of the DC conductivity plot can be expressed in the form [39].

3.7 Conductance spectra

The variation of conductivity as a function of frequency at different temperatures for PTh with stoichiometric ratio (70:30) wt% of thiophene and FeCl$_3$ is shown in Fig. 8. From the plot, it depicts that in the measured frequency range two distinct regions were observed, which is a low frequency plateau region where the conductivity helps understand weak frequency dependence and high frequency dispersion region where it increases rapidly. Moreover, the conductivity reveals dispersion with the increase of temperature, which shifts to higher frequency side (Table 2).

A convenient formalism to investigate the frequency behaviour of conductivity at room temperature is based on the power law proposed by Jonscher [40].

$$\sigma(\omega) = \sigma(0) + A\omega^n \qquad (3)$$

where $\sigma(\omega)$ is the total conductivity, $\sigma(0)$ is the frequency independent conductivity, A is a constant which determines the strength of polarizability and n is the power law exponent lying in the range $0 < n < 1$ that represents the degree of interaction between the mobile ions with the lattice around them. The conductivity data of all the samples of PTh with different stoichiometry of thiophene and FeCl$_3$ have been fitted to the above equation which shows good agreements with the experimental data.

The variation of imaginary part Z'' with frequency at different temperatures for PTh with (70:30) wt% of thiophene and FeCl$_3$ is plotted in Fig. 9. It is still remarkable that the imaginary part Z'' increases with frequency reaching a maximum peak value then decreases as the temperature increases. Moreover, the position of the relaxation peak shifts to higher frequencies with increasing temperature, in the same way, maximum peak values decrease. This shifting behaviour obeys the Arrhenius equation, which suggests that the ion transport follows the hopping mechanism [41].

The Fig. 10 depicts the frequency dependence plots of the real part of ε' at various temperatures for PTh with stoichiometric ratio of thiophene and FeCl$_3$ as (70:30) wt%. From the plot, it is clear that at a particular temperature the value of ε' decreases with increase in frequency that is the contribution from charge carriers towards the dielectric constant decreases with increase in frequency and attains a constant limiting value, which is not related to

Table 1 Advantages in the sense of properties of PTh under study over the referenced work

S.N.	Properties	Advantages
1.	Electrical	As-synthesized PTh shows conductivity at the order of 10^{-4} S cm^{-1}, hence such polymeric material has better performance in the field of optoelectronic and electronic devices
2.	Thermal	The thermal stability of PTh accomplished that this material is fit in the manufacturing of thermchromic devices, polymer electrode, sensor etc.
3.	Dielectric	The dielectric study of as-synthesized PTh reveals that such material is good for energy storage application such supercapacitors and battery application

Table 2 DC conductivity (σ), activation energy (E_a) for PTh with different stoichiometric ratios of thiophene and FeCl$_3$

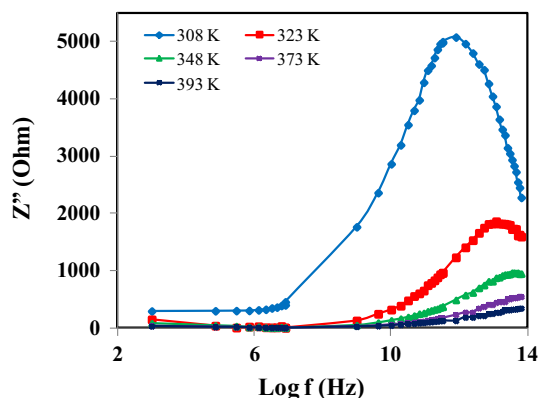| Sample	Conductivity (S cm^{-1}) at 303 K	Conductivity (S cm^{-1}) at 348 K	Activation energy (eV)
(90:10) wt%	8.42×10^{-6}	2.08×10^{-5}	0.23
(80:20) wt%	2.36×10^{-5}	4.93×10^{-5}	0.16
(70:30) wt%	1.09×10^{-4}	2.14×10^{-4}	0.14
(60:40) wt%	4.93×10^{-5}	1.09×10^{-4}	0.17
(50:50) wt%	3.07×10^{-5}	8.02×10^{-5}	0.19

Fig. 9 Plot of Z'' as a function of frequency and temperature for PTh with (70:30) wt% of thiophene and FeCl$_3$
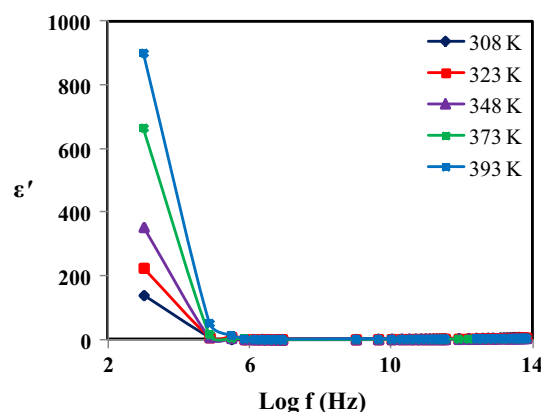

Fig. 10 Frequency and temperature dependence plot of real part of dielectric constant for PTh with (70:30) wt% of thiophene and FeCl$_3$

the hopping dynamics of mobile ions and may be due to the effect of rapid polarization process occurring in the sample. The high value of ε' in low-frequency region is a bulk phenomenon, which may be due to the presence of metallic or blocking electrodes which do not permit the mobile ions to transfer into the external circuit that is charge accumulation at the electrode-sample interface, as a result mobile ions pile up near the electrodes and give a large bulk polarization in the materials. In the high frequency region, at low temperatures, the well-known non-Debye behavior is observed [42, 43].

The variation of the normalized loss tangent with frequency at different temperature for PTh with stoichiometric ratio of thiophene: FeCl$_3$ (70:30) is shown in Fig. 11.

The tan δ increases with increase in frequency, attains maximum values, and thereafter decreases with increase in frequency. The frequency corresponding to the maximum value of tan δ was found to be shifted towards higher frequency side with raising temperature. The loss tangent peaks and their shift with temperature attribute to a dielectric relaxation process [44].

3.8 Modulus analysis

The modulus spectroscopy describes the bulk dielectric behaviour and dominates the effect of electrode polarization [42]. The electric modulus is described in terms of the reciprocal of the complex permittivity ε^*
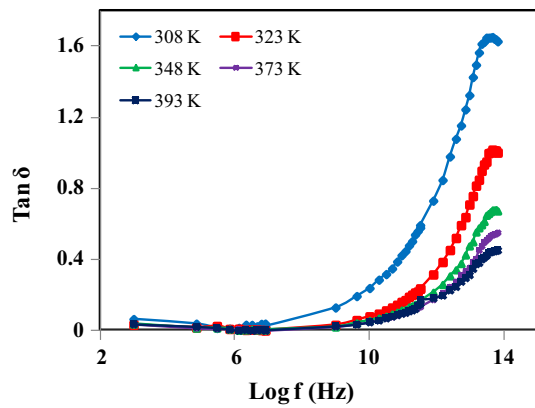
Fig. 11 Variation of tan (δ) versus log (f) for PTh with (70:30) wt% of thiophene and FeCl$_3$ for different temperature

$$M^*(\omega) = 1/\varepsilon^* = M' + jM'' \qquad (4)$$

where, M' is the real part and M'' is the imaginary part of the complex modulus M*(ω). From the complex modulus spectra, the conductivity relaxation can be analysed. Figure 12 represents M' versus M'' plot at different temperature for PTh with stoichiometric ratio of thiophene: FeCl$_3$ (70:30). The presence of an arc in the complex modulus spectrum concludes the single phase of the material. As seen in the plot, M' versus M'' spectra depicts that the semicircles are depressed and their centers are shifted down to the real axis, which confirms the distributions of relaxation time. This suggests the non-Debye type of relaxation in such material [45].

The variation of normalized modulus (M'/M'') versus Log ω at different temperatures for PTh with (70:30) wt% of thiophene and FeCl$_3$ display in Fig. 13. The plot depicts a long tail at lower frequency side, which is due to the large capacitance associated with the material. The shape of the spectrum remains constant but the position of the peak maxima is shifted towards the higher frequency side along
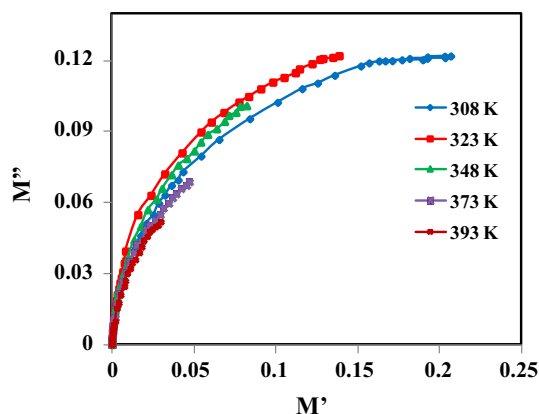

Fig. 12 Nyquist plot of electrical modulus for PTh with (70:30) wt% of thiophene and FeCl$_3$ for different temperatures
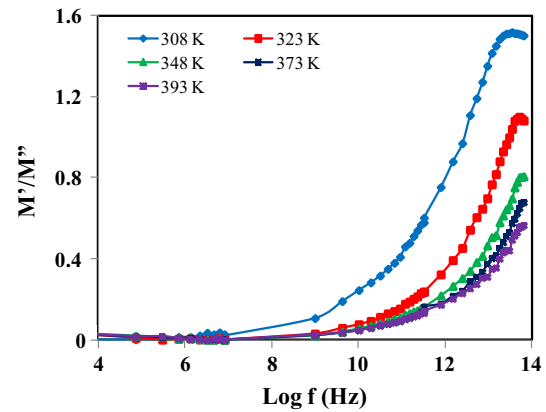

Fig. 13 Normalized modulus versus frequency plot for PTh with (70:30) wt% of thiophene and FeCl$_3$ for different temperatures
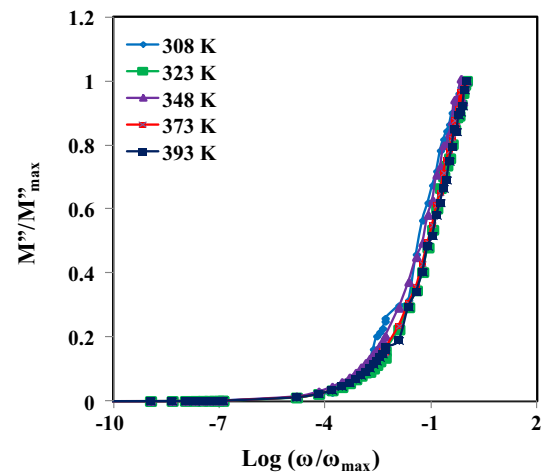

Fig. 14 Variation of M''/M''$_{max}$ with Log (ω/ω$_{max}$) for PTh with (70:30) wt% of thiophene and FeCl$_3$ at different temperatures

with the temperature. This behaviour concludes that the relaxation is thermally activated and hopping of charge carrier takes place. The asymmetric nature of the plots indicates a non-exponential nature of the conductivity relaxation. Hence there exists an asymmetric distribution of relaxation times [46].

M''/M''$_{max}$ versus Log (ω/ω$_{max}$) plots for PTh with (70:30) wt% of thiophene and FeCl$_3$ at different temperatures are shown in Fig. 14. All the curves merged into a single master curve, which indicates that relaxation mechanism is temperature independent. This phenomenon of relaxation mechanism is also reported by Cheruku et al. [47].

4 Conclusions

In the summary of present work, we successfully synthesized PTh by oxidative polymerization route using an oxidant FeCl$_3$. The principal bondings in PTh samples

properly assigned to specific groups. The polymer chain separation values of PTh samples were estimated using XRD analysis. TGA curve showed that PTh with (70:30) wt% of thiophene and $FeCl_3$ has more thermal stability than other. The DC conductivity shows Arrhenius-type temperature dependence. PTh with (70:30) wt% of thiophene and $FeCl_3$ showed the highest DC conductivity (1.09×10^{-4} S cm^{-1}) at 303 K and minimum activation energy (0.14 eV). The initial increase in conductivity with concentration of $FeCl_3$ may be due to increase in strength of the oxidizing agent, which increases the rate of polymerization. Thereafter, the conductivity decreases with increase in concentration of $FeCl_3$; because increasing $FeCl_3$ concentration may stiffen the polymer chains. The AC conductance spectrum obeys a Jonscher power law. The dielectric constant of the as-synthesized polymeric material decreases with increasing frequency and increases with increasing temperature. From the conductance and modulus spectra, it may be concluded that the charge carriers are unique, which are responsible for both conductivity and relaxation. Modulus analysis shows the non-Debye nature of polymer.

References

1. Z. Liu, L. Zhang, S. Poyraz, X.Y. Zhang, Curr. Org. Chem. **17**, 2267 (2013)
2. X.G. Li, M.R. Huang, W. Duan, Y.L. Yang, Chem. Rev. **102**, 2930 (2002)
3. M. Aydin, B. Esat, C. Kilic, M.E. Kose, A. Ata, F. Yilmaz, Eur. Polym. J. **47**, 2294 (2011)
4. J.I. Hong, I.H. Yeo, W.K. Paik, J. Electrochem. Soc. **148**, A163 (2001)
5. K.Y. Xie, J. Li, Y.Q. Lai, Z.A. Zhang, Y.X. Liu, G.G. Zhang, H.T. Huang, Nanoscale **3**, 2207 (2011)
6. B.H. Patil, A.D. Jagadale, C.D. Lokhande, Synth. Met. **162**, 1405 (2012)
7. B. Smitha, S. Sridhar, A.A. Khan, J. Membr. Sci. **225**, 76 (2003)
8. X.J. Wang, M.R. Andersson, M.E. Thompson, O. Inganas, Synth. Met. **137**, 1020 (2003)
9. F. Bloisi, A. Cassinese, R. Papa, L. Vicari, V. Califano, Thin Solid Films **516**, 1598 (2008)
10. C.N. Kotanena, A.N. Wilson, C. Dong, C.Z. Dinud, G.A. Justina, A.G. Elie, Biomaterials **34**, 6327 (2013)
11. H.S. Nalwa, *Handbook of Organic Conductive Molecules and Polymer* (Wiley, New York, 1997)
12. Q.T. Vu, M. Pavlik, N. Hebestreit, J. Pfleger, U. Rammelta, W. Plieth, Electrochim. Acta **51**, 1124 (2005)
13. G.C. Arteaga, M.A. del Valle, M. Antilén, F.R. Díaz, M.A. Gacitúa, P.P. Zamora, J.C. Bernède, L. Cattin, G. Louarn, Int. J. Electrochem. Sci. **7**, 7854 (2012)
14. L.R. Chen, L.Z. Ping, Chin. Sci. Bull. **54**, 2032 (2009)
15. J.W.P. Lin, L.P. Dudek, J. Polym. Sci. Polym. Chem. **18**, 2873 (1980)
16. S.V. Kamat, S.H. Tamboli, V. Puri, R.K. Puri, J.B. Yadav, O.S. Joo, Arch. Phys. Res. **1**, 122 (2010)
17. N. Ballav, M. Biswas, Mater. Sci. Eng., B **129**, 272 (2006)
18. J.M. Pringle, M. Forsyth, D.R. MacFarlane, K. Wagner, S.B. Hall, D.L. Officer, Polymer **46**, 2058 (2005)
19. M.G. Voronkov, I.A. Tokareva, I.A. Dorofeev, V.I. Smirnov, L.G. Shagun, Russ. J. Gen. Chem. **80**, 2079 (2010)
20. D. Reyman, E. Guereca, P. Herrasti, Ultrason. Sonochem. **14**, 665 (2007)
21. J.M. Lee, S.J. Lee, Y.J. Jung, J.H. Kim, Curr. Appl. Phys. **8**, 663 (2008)
22. D.S. Kelkar, A.B. Chourasia, Indian J. Phys. **86**, 107 (2012)
23. I. Imae, S. Imabayashi, K. Korai, T. Mashima, Y. Ooyama, K. Komaguchi, Y. Harima, Mater. Chem. Phys. **131**, 756 (2012)
24. A. Gok, M. Omastova, A.G. Yavuz, Synth. Met. **157**, 29 (2007)
25. D.S. Kelkar, A.B. Chourasia, *Macromolecular Symposia, Special Issue: Nanostructured and Biorelated Materials*, vol 327 (2013), p. 53
26. B.Z. Lin, C. Ding, B.H. Xu, Z.J. Chen, Y.L. Chen, Mater. Res. Bull. **44**, 723 (2009)
27. H. Higashimura, S. Kobayashi, *Encyclopedia of Polymer Science and Technology, oxidative Polymerization* (Wiley, New York, 2004)
28. Y. Ding, A.B. Padias, H.K. Hall, J. Polym. Sci., Part A: Polym. Chem. **37**, 2579 (1999)
29. M.R. Karim, K.T. Lim, C.J. Lee, M.S. Lee, Synth. Met. **157**, 1012 (2007)
30. S. Richard, P. Gnanakan, M. Rajasekhar, A. Subramania, Int. J. Electrochem. Sci. **4**, 1301 (2009)
31. R.E. Partch, S.G. Gangoli, E. Matijevic, W. Cai, S. Arajs, J. Colloid Interface Sci. **144**, 34 (1991)
32. S.A. Waghuley, S.M. Yenorkar, S.S. Yawale, S.P. Yawale, Sens. Actuators, B **128**, 373 (2008)
33. B. Sari, M. Talu, F. Yildirim, E.K. Balci, Appl. Surf. Sci. **205**, 38 (2003)
34. D.S. Kelkar, A.B. Chourasia, J. Chem. Chem. Tech. **5**, 309 (2011)
35. A. Mhamdi, B. Ouni, A. Amlouk, K. Boubaker, M. Amlouk, J. Alloys. Compd **582**, 822 (2014)
36. S. Sahoo, U. Dash, S.K.S. Parashar, S.M. Ali, J. Adv. Ceram. **2**, 300 (2013)
37. M.B. Armand, J.M. Chabagno, M.J. Duclot, in *Fast Ion Transport in Solids*, ed. by P. Vashista, J.N. Mundy, G.K. Shenoy (Amsterdam, North Holland, 1979)
38. N. Reddeppa, A.K. Sharma, V.V.R. Narasimha Rao, W. Chen, Measurement **47**, 41 (2014)
39. A.A. Assencia, C. Mahadevan, Bull. Mater. Sci. **28**, 418 (2005)
40. M.H. Lakhdar, B. Ouni, M. Amlouk, Mater. Sci. Semicond. Process. **19**, 39 (2014)
41. B.B. Mohantya, P.S. Sahoo, M.P.K. Sahoo, R.N.P. Choudhary, Adv. Mater. Lett. **4**, 308 (2012)
42. A. Dutta, T.P. Sinha, P. Jena, S. Adak, J. Non Cryst. Solids **354**, 3957 (2008)
43. S. Jayaseelan, P. Muralidharan, M. Venkateswarlu, N. Satyanarayana, Mater. Chem. Phys. **87**, 377 (2004)
44. D. Ravinder, A.V.R. Reddy, G.R. Mohan, Mater. Lett. **52**, 265 (2002)
45. B.G. Soares, M.E. Leyva, G.M.O. Barra, D. Khastgir, Eur. Polym. J. **42**, 686 (2006)
46. Y. Xi, Y. Bin, C.K. Chiang, M. Matsuo, Carbon **45**, 1309 (2007)
47. R. Cheruku, L. Vijayan, G. Govindaraj, Mater. Sci. Eng., B **177**, 779 (2012)